Superlattices of Platinum and Palladium Nanoparticles

James E. Martin, Jess P. Wilcoxon, Judy Odinek, and Paula Provencio
Sandia National Laboratories
Albuquerque, New Mexico 87185-1421

Abstract

We have used a nonionic inverse micelle synthesis technique to form nanoclusters of platinum and palladium. These nanoclusters can be rendered hydrophobic or hydrophilic by the appropriate choice of capping ligand. Unlike Au nanoclusters, Pt nanoclusters show great stability with thiol ligands in aqueous media. Alkane thiols, with alkane chains ranging from C_6 to C_{18} were used as hydrophobic ligands, and with some of these we were able to form 2-D and/or 3-D superlattices of Pt nanoclusters as small as 2.7 nm in diameter. Image processing techniques were developed to reliably extract from transmission electron micrographs (TEMs) the particle size distribution, and information about the superlattice domains and their boundaries. The latter permits us to compute the intradomain vector pair correlation function of the particle centers, from which we can accurately determine the lattice spacing and the coherent domain size. From these data the gap between the particles in the coherent domains can be determined as a function of the thiol chain length. It is found that as the thiol chain length increases, the gaps between particles within superlattice domains increases, but more slowly than one might expect, possibly indicating thiol chain interdigitation.

Sandia is a multiprogram laboratory operated by Sandia Corporation, a Lockheed Martin Company, for the United States Department of Energy under contract DE-AC04-94AL8500. This work supported by the Division of Materials Sciences, Office of Basic Energy Sciences, U.S. Department of Energy (DOE).

DISCLAIMER

Introduction

There has been considerable recent interest in the formation of superlattices of metal nanoclusters synthesized by solution or gas phase methods. Most of this work has focused on Au nanoclusters, because this metal readily forms reasonably monodisperse spherical particles that when coated with some alkanethiols readily order into superlattices upon solvent evaporation. In this paper we investigate the synthesis of platinum and palladium nanoclusters in inverse micelle solutions, and demonstrate the formation of superlattices of these materials. Superlattice formation with Pt and Pd is more difficult than Au, because of the tendency of these nanoclusters to grow as highly faceted single crystals. However, under the appropriate synthetic conditions, and in some instances by allowing the nanoclusters to ripen at room or elevated temperatures, it is possible to grow narrow dispersity nanoclusters of these catalytic metals that form superlattices. These nanoclusters can be capped with both hydrophilic and hydrophobic ligands, and we used quasielastic light scattering to determine which of these results in nanoclusters that are dispersed at the single particle level.

To investigate the issue of gap control, we capped Pt nanoclusters with alkane thiols having a range of chain lengths. We found that many, but not all, of these thiols facilitate superlattice formation. However, a number of unexpected parameters affect the results, including amount of time between reduction and capping, the choice of oil used to form micelles, the specific reducing agent, etc. To quantify the gaps between particles we used image processing techniques that can compute a variety of parameters from TEM images of 2-D particle arrays. In addition to the particle size distribution, particles are classified as to whether or not they are in an ordered domain, and the crystalline domains are enumerated so that the coherent intradomain vector pair correlation function can be computed. This provides a precise determination of the lattice spacing and the coherence length in the superlattices, and combining this with the average particle size allows a precise determination of the particle gaps, which do indeed increase with the alkane thiol chain length.

Background

The history of the surfactant-based synthesis of metal nanoclusters starts with the seminal 1982 paper of Boutonnet, Kizling, Stenius, and Maire, [1] who used two inverse micelle forming systems: 1) the nonionic surfactant pentaethylenegylcol dodecyl ether in hexane and; 2) the cationic surfactant cetyl trimethylammonium bromide (CTAB), in octanol. The metal salts used were H_2PtCl_6, $PdCl_2$, $RhCl_3$, and $IrCl_3$, these metals being chosen for their catalytic potential. The successful preparations of Pt nanoclusters are illustrative. In the cationic surfactant case, the inverse micelles were swollen with a dilute, ~ 8 mM aqueous H_2PtCl_6 solution, to form inverse microemulsions with aqueous phase loadings of about 14 wt%. In the nonionic surfactant case, the inverse micelles were swollen with a concentrated, ~ 1.2 M aqueous H_2PtCl_6 solution, to form inverse microemulsions with aqueous phase loadings of about 0.3 wt% and Pt ion concentrations of 4 mM. These precursor solutions were then reduced with hydrazine to form a stable dispersion of ~3 nm Pt nanoclusters.

The use of water restricts the synthesis of metal nanoclusters to inert metals which are not easily oxidized. In 1989 it was demonstrated [2,3] that the synthesis of metal nanoclusters could be done in inverse micelle solutions, by directly dissolving the metal salt into an oil containing certain types of surfactants that spontaneously aggregate to form droplet-like micelles with nanometer dimensions and hydrophilic interior regions. This method was shown to give more monodisperse nanoclusters than those produced by a microemulsion synthesis using the nonionic poly(ethyleneglycol) alkyl ether surfactants. A typical synthesis uses the nonionic surfactant penta(ethyleneglycol) dodecyl ether in octane and the metal salt $NaAuCl_4$. This inverse micelle synthesis also permits the use of strong reducing agents, such as $LiBH_4$, which hydrolyzes in water. Using this technique, nanoclusters of easily oxidizable metals, such as Fe, can be produced [4].

To our knowledge, the first mention of the formation of Au nanocluster superlattices is the 1993 paper by Giersig and Mulvaney [5], who synthesized Au nanoclusters by the aqueous Turkevich method [6], in which $AuCl_4^{-1}$ is reduced by sodium citrate. These 14 nm diameter, negatively charged clusters were deposited onto a

TEM grid by application of a 10-100 mV potential, forming monolayer arrays of large extent. The gap between these particles was 1.0 nm, consistent with the size of the citrate ion stabilizer.

A number of other investigations of Au nanoclusters and their spontaneous assembly into superlattices have been reported, following an inverse micellar synthesis reported by Brust et al. [7], using the cationic surfactant tetraoctylammonium bromide in toluene. In this method, salt addition is indirect, accomplished by dissolving the metal salt in water, and then extracting the metal salt alone into the inverse micelle solution. In this work, and those that followed, [8-13] clusters are capped with dodecanethiol, which facilitates superlattice formation and can be used to limit cluster growth. Brust later reported [14] the formation of superlattices of 8 nm Au nanoclusters crosslinked with dithiols, specifically, 1,12 dodecanedithiol and *p*-xylenedithiol. Andres et al. [15] demonstrated the formation of Au nanocluster superlattices from particles synthesized by a gas phase technique and stabilized by a dodecanethiol mist. The clusters formed conducting arrays when linked by aryl dithiols or aryl di-isonitriles. Studies of Pt nanocluster arrays are limited to the work of Sarathy et al., [11] who were able to form arrays of limited coherent domain size with dodecanethiol capped Pt nanoclusters.

One group has reported a study of the interparticle separation with metal (Au) nanoclusters functionalized with a family of ligands of variable chain length [16]. They employed the inverse micelle synthesis technique, using the tetraalkylammonium bromide ($NR_4^+Br^-$) family of cationic surfactants with R varying from C_6 to C_{18} in toluene. [17] An analysis of TEM images, using a graticule, gave a smaller than expected increase of 1.27 Å per carbon atom of the particle spacing on the chain length of the surfactant. It is mentioned that the cluster size distribution was affected by the choice of surfactant, but no analysis of the average cluster size was reported, so the effect of surfactant chain length on the particle gaps cannot be addressed.

Experimental

Synthesis. The nanoclusters are synthesized in inverse micelles, by directly dissolving the metal salt, to a concentration of 0.01 M, into an anhydrous, 10% solution of surfactant

in oil. Dissolution occurs overnight with vigorous stirring in a light-shielded container. Reduction is carried out under Argon in a Vacuum Atmospheres™ glovebox. The molar ratio of reducing agent to metal salt, *R*, and is listed in **Tables I&II**, and is typically 4. The reacted solution is removed from the glovebox and the clusters are stabilized by capping with an alkanethiol or other suitable capping agent at least one hour after chemical reduction, but sometimes as long as one day or even one week. The stabilized clusters are then purified. Under appropriate conditions, monodisperse clusters form that do not require fractionation to form superlattices with large coherent domains.

We use nonionic surfactants having a polyether headgroup attached to a linear hydrocarbon tail. These surfactants are designated by the nomenclature C_iE_j where i is the number of CH_x units in the alkyl chain and j equals the number of ether groups, e.g. $C_{12}E_5$ denotes penta(ethyleneglycol) mono n-dodecyl ether. In our syntheses i = 12 and j is in the range of 4 to 8. The ultrapure nonionic surfactants we use are obtained from Nikko chemicals, Japan. $C_{12}E_5$ is most often chosen, due to the ease with which it can be extracted into NMF.

A range of oils are used, including pentane, hexane, octane, decane, dodecane, and hexadecane, depending on the application. The oil can have an effect on the nanoparticle size and dispersity. Pentane and hexane, because of their higher volatility, are used when samples are prepared for thin film formation. The high alkanes are chosen for superlattice formation and dielectric studies. The alkanes decane and higher are easily rendered ion free by extraction with deionized water.

A variety of metal salts were used to produce Pt and Pd nanoclusters, including hydrogen hexachloroplatinate (IV) hydrate, sodium hexachloroplatinate (IV) hydrate, and sodium tetrachloropalladate (III) hydrate. The choice of salt can be used to obtain some degree of size control.

The reducing agents used in the studies reported here are lithium aluminum hydride, lithium borohydride, and lithium triethylborohydride (Super-Hydride®). The choice of the reducing agent is a primary determinant in the quality of the nanoclusters, as is the manner in which it is introduced into the solution. Predilution of some of the reducing agents to 0.2 M with tetrahydrofuran or toluene causes a rapid reaction and

results in much smaller nanoclusters, due to the high density of nucleation sites thus produced.

Alkanethiols of various chain lengths were dissolved in decane to a 0.5 M concentration. These alkanethiols were added to the nanocluster solutions to give a final concentration of 0.01 M. In general, we found that the thiols with chains of 6 carbons or shorter resulted in the precipitation of the nanoclusters, in the form of superlattice crystallites. Likewise, samples capped with the longer chain thiols ($C_{16}SH$, $C_{18}SH$) precipitated, but not as quickly. Thus the ability to control the particle gaps in superlattices is limited by the observed stability window.

Purification. To purify the nanoclusters several approaches were used; liquid phase extraction, precipitation, and solid phase extractors. Before surfactant extraction from the inverse micellar solutions containing the nanoclusters, the nanoclusters are first rendered hydrophobic by capping the cluster surface with alkane thiols, designated C_kSH, where $3<k<18$ denotes the length of the alkane group. Longer chain alkyl thiols, with $k\geq 8$, are the most effective.

Liquid phase extraction is effective at removing the surfactant from samples prepared in simple alkanes, since alkanes are immiscible in polar organic solvents in which the surfactants are highly soluble, while the alkanethiol capped nanoclusters are highly insoluble in polar solvents. This method has the advantage of keeping the nanoclusters dispersed throughout the process. Investigations of a wide variety of extractants showed that n-methylformamide (NMF), with its high dielectric constant of 189, effectively extracts all the ionic by-products and most of the surfactant from thiol stabilized nanoclusters, even for the surfactant $C_{12}E_4$, which has a short polyether tail. Partitioning ratios exceed 100:1 for all surfactants used, so three extractions is more than adequate. (The most likely extractant - water - is ineffective at surfactant extraction.) NMF is slightly soluble in lower alkanes, but can be subsequently removed by extractions with deionized water. Excess thiol capping agent is extracted with a 0.1 mM NaOH solution. The samples can be chilled and the oil phase conveniently decanted.

Precipitation with a non-solvent is a conventional method of nanocluster purification that is effective for nanoclusters prepared in toluene. Unlike liquid

extraction, it cannot be used with nanoclusters prepared in alkanes, since the polar, organic non-solvents like methanol, ethanol or acetone used to precipitate the hydrophobic alkanethiol stabilized nanoclusters from solution are immiscible in alkanes. Precipitation can cause stability problems, however. A second precipitation can wash the capping ligands off the clusters, leading to aggregation and even the formation of a metal film on the glass vial. And metal nanoclusters do not precipitate a second time without aggressive centrifugation, which tends to compact the nanocluster pellet to such a extent as to render resuspension in non-polar solvents almost impossible.

Solid-phase extraction cartridges are available (e.g. Water's corp. Sep-Pak) containing the same types of materials used in HPLC columns. These disposable cartridges of organically functionalized silica, alumina or ion exchangers are able to retain polar or ionic materials while passing non-polar ones like alkanethiol stabilized metal nanoclusters. They are commonly used to concentrate analytes by large amounts prior to chemical analysis, but we have found they also work well for purifying nanoclusters. The final nanocluster solution purity after two to three passages through the cartridge is quite good, as demonstrated by HPLC analysis.

Nonionic inverse micelle surfactants become nearly insoluble at low temperatures, and so can be crystallized out of solution. For example, the solution **Pt 53J**, made from C12E5/decane/Na_2PtCl_6/$LiBH_4$/1-mercapto-2-propanol, was iced, causing the surfactant to crystallize, and centrifuged for 5 min at 966 g at 0°C. A whitish surfactant pellet - free of nanoclusters - formed. The supernatant was poured into another tube and spun again at –10°C for 5 min. without pellet formation, indicating no further surfactant removal. In another case, **Pt 76**, C12E4/decane/Na_2PtCl_6/$LiBH_4$, which had no surface stabilization, was spun for 5 min at 966 g in a –10°C precooled centrifuge. A white pellet formed. This did not happen with **Pt 53D**, prepared identically to **Pt 53J** except for the capping agent (3-mercaptopropionic acid). Instead, the sample coagulated and did not form a distinct pellet when centrifuged under identical conditions as **Pt 76**. With **Pt 78D**, C12E4/decane/Na_2PtCl_6/$LiBH_4$/dodecanethiol, a 5 minute spin produced no pellet. A second 5 minutes resulted in a white pellet, but over one half of the sample spun out into a brown pellet when an additional 5 minutes was added to the process.

Similar processing was tried with other solutions but this method was not pursued further because of the success and simplicity of the liquid phase extraction method.

Annealing. Aging the nanocluster solutions often leads to reduced polydispersity. Significant sample aging at room temperature takes weeks or months, so we decided to determine whether thermal annealing could reduce this time. Studies were conducted on **Pd 149**, for which a sample held at ambient for ten days is shown in **Fig. 1**. Image analysis yields an average cluster size of 3.9nm±25%, and this large polydispersity prevents array formation. When this sample is held at ambient temperature for 80 hours, then aged at 70°C for 96 hours, the cluster size increases to 5.6nm±16%, and the reduced polydispersity leads to marginal array formation, **Fig. 1**. With an optical microscope we saw the first 3-d crystals that were grown from palladium from this particular sample, demonstrating that thermal annealing can be effective.

Results

Spherical nanoparticles. The primary difficulty encountered with platinum is the tendency for clusters to form with highly faceted surfaces, as shown in the case of **Pt 78** in **Fig. 2**. These non-spherical particles are actually single crystals, as the lattice fringes observed in high resolution TEM indicate. The formation of faceted particles frustrates the formation of periodic arrays, instead leading to the formation of the mosaic structures shown in **Fig. 3**. In this mosaic of **Pt 119** nanoparticles one can observe many strings of stacked rectangular particles, and it is quite possible that the structure formation in this mosaic is entropically driven, essentially due to the tendency of the hard particles to achieve a densely packed state in a region having a contracting boundary, due to solvent evaporation. Of course, it is also possible that thiol chain interactions play a role, due to a tendency to interdigitate. This would tend to maximize the total length of narrow particle gaps, which is also a feature of this mosaic. Simulation studies of the packing of ellipsoids show similar features [18].

We do not understand the factors that lead to the formation of faceted particles, but in studies of two-dimensional epitaxial growth the factors that control island

morphology are the rate of atom deposition, the diffusivity of surface atoms, the sticking probability of surface atoms onto the island edges, the edge mobility of atoms, and the dependence of the island energy on morphology. Fractal-like structures occur when the time scale of island formation is fast compared to the timescale to relax to a minimum free energy structure. Similar considerations should apply to nanoclusters, and rough surfaces on Pt nanoclusters might correspond to a low surface atom mobility on these relatively large particles, a reasonable assumption for an element with such a high melting temperature.

The dominant formation mechanism for these nanoclusters is probably particle-cluster growth. This is reasonable since we know that the number of Pt salt molecules per inverse micelle is extremely small (<50 Pt atoms) before chemical reduction, compared to the number of atoms in a nanocluster after reduction (~4,300 for a 5.0nm diameter Pt particle). One possible description of the synthetic process is that the reducing agent, after being mixed into the solution, diffuses into the inverse micelles, effecting the reduction of a Pt atom. A reduced Pt atom will then attach itself to any available nucleated nanocluster, either by free diffusion through the oil phase, or by surfactant moderated diffusion, in the form of a partial or complete inverse micellar structure. If the surface mobility on the nanoclusters is high, so that extensive restructuring can occur on the timescale of surface diffusion, then one can expect particle morphologies to evolve that minimize the cluster energy in the surfactant rich environment. Because the cluster melting temperature is a strong function of particle size, one might reason that smaller particles might tend to have morphologies that are closer to an energy minimum for their size. Small particle size is favored by an increase in the density of nuclei, which in turn is favored by a rapid (chemical) quench into the two phase region.

We have found that the rate of chemical reduction is greatly increased by the predilution of the reducing agent into THF, which is completely soluble into the oil phase. In fact, predilution of the reducing agent in this way produces a violent reaction, with lots of exciting gas formation etc. The result is a tremendous number of nuclei, and the formation of lots of small nanoparticles. This is exactly the reverse of the well-known process for growing large particles, whereby small particles are first formed, and

subsequently enlarged by heterogeneously nucleating a slowly added reagent, trying to avoid supersaturation in the solution, and further homogeneous nucleation. An example of this is the 4.0nm±10% **Pt 98A** nanoclusters in **Fig. 4**, which although not as stunning as a good Au sample, nonetheless have a sufficiently low dispersity that superlattice formation occurs on a TEM grid. Also shown is the computed *intradomain* vector pair correlation function of the particle centers of mass, a process that is described fully in the Appendix. Briefly, this function is obtained from image processing of the full TEM image, and contains contributions only from particles within hexagonal domains. Contributions from separate domains are added coherently, by domain rotation. The Fourier transform of this function is the single domain electron diffraction pattern divided by the particle structure factor. Precise estimates of the lattice spacing, necessary for the determination of particle gaps as a function of the alkanethiol chain length, are facilitated by this correlation function. Also computed from the TEM image is the distribution of particle diameters, shown for **Pt 98A** in **Fig. 5**. This automated analysis is also described in the Appendix. As with any technique, this process has a resolution limit. The resolution limit depends in a complex way on the image quality, but in any case, the estimates of the width of the size distribution we quote will be overestimates of the true polydispersity.

Superlattice formation. Using the same predilution of the reducing agent technique, but with a different reducing agent, we produced the 2.7nm±10% **Pt 165** nanoclusters shown in **Fig. 6**. These clusters contain ~700 Pt atoms. Of course, even the method of addition of reducing agent is a significant factor determining the density of nuclei, and this is only moderately controlled. These nanoclusters are clearly single domain, as indicated from the appearance of lattice fringes, and appear to be reasonably spherical. With this sample, superlattice formation occurs very readily, with some interesting effects. It is well documented that in bilayers of alkanethiol capped Au nanoclusters, particles occupy the two-fold saddle sites, forming string-like structures that sometimes loop. We have observed this as well, **Fig. 7**. Surprising in light of this is that in bilayers of alkanethiol capped Pt nanoclusters, the particles occupy the three-fold saddle sites. One can only imagine that this difference is due to the relative interactions of the alkane chains with the

cluster surface and each other. The particle size is also quite different in these cases, but this does not appear to be the controlling factor, since the occupation of two-fold saddle sites is observed for Au arrays of widely varying particle sizes..

The coherent domain size can be quite large in 3-D superlattices of **Pt 165**, as indicated in the TEM of part of a single domain, **Fig. 8**. The selected area diffraction pattern is included in this figure, and shows well-resolved hexagonal peaks, indicative of a large coherent single domain.

Annealing is another route to the production of monodisperse Pt nanoclusters. The sample **Pt 58A** was capped with dodecanethiol and annealed for six months at room temperature, yielding a solution of 4.6nm±8% particles, **Fig. 9**. The size distribution for this sample is as narrow as that of a good Au sample, and superlattices are easily formed. However, in addition to the expected hexagonal arrays, we very often observe square lattices, **Fig. 10**, which we find extraordinary.

Superlattice crystals. To form macroscopic superlattice crystals, an aliquot of the solution is deposited on a substrate and allowed to evaporate slowly by adding a nonvolatile solvent, such as dodecane, at 25 vol. %, and/or by covering the solutions with a Petri dish. Various substrates we tried, including graphite, paraffin, Mylar, Teflon, natural mica, glass, silicon, and lanthanum aluminum oxide. Graphite was too porous, and paraffin is not compatible with clusters suspended in oils. Our first 3-D crystals were successfully grown on a glass substrate, but other substrates proved better, especially Teflon™, since the high interfacial tension prevents wetting, which results in a low surface area for solvent evaporation, encouraging the formation of large crystals. The first Pt nanocluster superlattice crystals were grown on silicon from **Pt 58A**, and are shown in **Fig. 11** as both an optical micrograph and an SEM image. The exact conditions determine the crystal morphology to some extent, as the crystals in **Fig. 12** show, which have a dendritic appearance. Other Pt samples from which good crystals were formed include **Pt 160**, **Pt 161**, and **Pt 162**, but none of these were as high in quality as the annealed **Pt 58A** sample.

Finally, for Pt samples made by all methods tried, we found that it is important to allow the solution to age for 24 hours before adding the thiol capping agent. Capping too

soon causes nanocluster aggregation and sedimentation. HPLC studies demonstrate that over this 24 hour aging period there is a considerable decrease in the cluster size distribution, accompanied by significant cluster growth. At this time we do not understand the conditions of the cluster surface that are essential to successful capping with alkane thiols.

Finally, we were also successful in growing superlattice crystals of Pd, as shown in **Fig. 13**. These crystals are much lower in quality than the Pt crystals. As previously discussed, palladium nanoclusters are much like Pt - difficult to make spherical and monodisperse. We were successful using the nonionic surfactant C12E5 in hexadecane, with lithium borohydride as the reducing agent, and sodium tetrachloropalladate (III) hydrate as the Pd salt. The molar ratio of reducing agent to metal salt was 4:1. Pd QDAs are also discussed in the section on thermal aging.

Control of interparticle gaps. To explore the control of interparticle spacing on thiol chain length we capped a Pt nanocluster solution with thiols from C_6SH to $C_{18}SH$ in steps of even carbon numbers. The solution with C_6SH immediately precipitated, solutions capped with C_8SH, $C_{10}SH$, $C_{12}SH$, and $C_{14}SH$ remained stable, and solutions capped with $C_{16}SH$ and $C_{18}SH$ slowly precipitated.

These solutions were immediately deposited on holey carbon grids, and TEM images of the superlattices were collected in a single day, to minimize aging effects. Nanoclusters capped with C_8SH to $C_{18}SH$ show reasonably ordered 2-D lattices, indicating that the clusters remain fully dispersed in solution until the solvent evaporates on the grid. Nanoclusters capped with C_6SH do not form ordered 2-D arrays.

Using the software described in the Appendix, the radial pair correlation functions of the superlattices were determined, using the convolution method. From this function the lattice spacing was then determined. The dependence of the average nanocluster size on the thiol chain length is shown in **Fig. 14**. Fitting these data gives an increase in the particle gap of 1.4Å per carbon atom, which is roughly half that expected from HPLC studies of the capped nanoclusters in solution. The thiol chains either collapse somewhat upon solvent evaporation, or tend to interdigitate. These results are very similar in magnitude to that obtained for Au, the primary difference being Au does not form

superlattices with $C_{16}SH$ and $C_{18}SH$, due to the large nanoparticle dispersity that results from the addition of these thiols to Au nanocluster solutions.

Hydrophilic ligands. Although the main focus of these investigations is superlattice formation, some investigations were made into rendering the surface of Pt nanoclusters hydrophilic. This can be advantageous if one wishes to incorporate these nanoclusters into other periodic media, such as surfactant-templated mesoporous silica, which is synthesized in polar liquids, e.g. water/n-methylformamide mixtures. 0.5M solutions of the capping ligands listed in **Table III** were prepared in the listed solvents and added to Pt nanoclusters to give a final concentration of 0.10 M. Aliquots of the capped Pt nanoclusters in oil/surfactant were then precipated with 1-propanol. The clusters were spun down, the supernatant was decanted, and the cluster precipitate was resuspended in 1-propanol. This precipitation process was repeated several times, and clusters were then redissolved in a variety of hydrophilic solvents.

Quasielastic light scattering (QELS) was used to determine the efficacy of the various capping ligands in stabilizing the clusters. In this scattering technique the hydrodynamic radius of the nanoclusters, or aggregates thereof, is determined. Solutions containing large aggregates are not deemed successfully redispersed, whereas those that demonstrate a hydrodynamic radius close to that of a single nanocluster are evidently dispersed at nearly the single particle level, which is the desired result. In fact, successful redispersion of Pt nanoclusters can *only* be assessed with QELS because even though a nanocluster solution might be stable and appear very good to the naked eye, substantial particle aggregation may have occurred. With quasielastic light scattering we are able to determine precisely the hydrodynamic radius of the clusters and only if the results obtained were consistent with nanocluster sized particles is the redispersion given as successful for the three solvents listed in **Table III**.

Conclusions

We have shown that Pt nanoclusters grown in inverse micelles have a tendency to develop faceted surfaces which mitigate against superlattice formation. Under the

appropriate reaction conditions, however, it is possible to form roughly spherical Pt nanocluster solutions of reasonably low dispersity that form superlattices on a TEM grid, and that crystallize well. One of the interesting differences between Pt and Au nanoclusters is that bilayers of Pt nanoclusters show stacking in the three-fold saddle sites, whereas Au stacks anomalously in the two-fold saddle sites. Another unusual feature in Pt, is the frequent formation of square lattices on a TEM grid. The interparticle spacing of Pt superlattices can be controlled over a limited range by capping with alkanethiols. The lattice spacing increase by ~1.4Å per carbon atom in the alkanethiol chains in the range of 8-18 carbons. Pd nanoclusters grown in inverse micelles tend to be very polydisperse, but thermal annealing at 70°C reduces the dispersity sufficiently that crystals can be formed. Finally, investigations of hydrophilic ligands show that Pt nanoclusters can be dispersed at the single particle level in hydrophilic solvents, and remain stable indefinitely.

Appendix - Image Analysis

Nanoclusters that form superlattices are different from molecules that form crystals in that a significant size distribution occurs. A large size distribution can prevent the formation of large coherent domains and in extreme cases even prevent crystallization. To obtain information such as the coherent domain size from molecular crystals, one uses x-ray or neutron diffraction, where such properties are computed from the linewidth. The interpretation of the linewidth of the superlattice reflections is not as clear, since it is affected by both crystalline domain size and cluster polydispersity. The crystalline domain size can be large, but the translational symmetry of the superlattice is stillcompromised by polydispersity, with the smaller clusters tending to crystallize at the edge of the domain.

Fortunately, nanoclusters are sufficiently large that real space data in the form of TEM images are easily obtained, and these contain information that is directly accessible. To this end we have developed software that enables the accurate determination of many of the parameters associated with 2-D superlattices. In the following is a description of the information that can be obtained, as well as a brief description of the algorithms.

Cluster positions. The first step in image analysis we call FindClusters. This primary goal of this program is to accurately determine the size, shape, and center of mass position of all the acceptable nanoclusters in a TEM image. Distribution functions of cluster mass, radius, etc. can then be computed, as well as moments of these distributions. The radial pair correlation function of the particle centers of mass are also computed, and a file of particle coordinates is created for further analysis.

In the first stage of this program we attempt to make clear distinction between the nanoclusters and the TEM holey carbon grid. The image is first processed so that the grayscale values of the pixels indicating particles exceed those of all of the pixels indicating the grid. The image can then be thresholded to a binary image wherein all of the particle pixels have the maximum grayscale value of 255, and the grid pixels have a grayscale value of 0. We approach this problem by two methods, convolution and conditional thresholding.

In the first approach the image is convoluted with an operator that is roughly the second derivative of a Gaussian. The integral of this 2-D function is zero in the plane, so when applied to a uniform region of the image, a zero result is obtained. The convolution is done point-wise, with global update, and when the radius of the convolution operator is appropriately chosen so that the positive part of the function just covers the particles, the resulting processed image shows readily discernable boundaries around diffuse particles, and is readily thresholded. The convolution approach is only useful for determining the particle centers, since particle size information is obliterated by the operator, and is most effective when the polydispersity is not too large. But convolution works well even for very poor images where the conditional thresholding approach fails.

When particle size information is required, a different approach is taken. First, the image is moderately smoothed, by replacing each pixel value by an unweighted average of itself and the average of its neighbors. Then a conditional thresholding technique is applied, whereby a pixel is set to 255 if its value exceeds a selected threshold value *and* 40% of its 8 nearest neighbors exceed that value. This insures that noise from the grid does not appear as small particles. The result of these operations is an effectively thresholded image.

Particle size determination. The next task is the efficient enumeration and quantification of the particles. To accomplish this, each pixel is assigned a unique identifying number. The image array is then repeatedly scanned, and each pair of neighboring pixels that are assigned the grayscale value 255 have their pixel IDs changed to that of the lower ID of the pair. The image is scanned until no further ID changes occur. The result of this is that every connected cluster of black pixels consists of pixels with the same ID. No two disconnected clusters will have the same ID. It is now simple to compute the areas of all the clusters, and their projected radii of gyration - the root mean square separation of the pixels from their center of mass. Also, the ratio of their area to their radius of gyration is computed, which is a maximum for round clusters.

Particle discrimination. The next stage of processing is discrimination. Not every resolved feature should be counted as a cluster. For example, overlapping particles should be excluded, as well as those particles that contact a border of the image. In some cases it may be desirable to delete features of the image that are too small, too large, or unusual in shape. These criteria can be selected by setting various discrimination gates.

The accepted particles are now analyzed. Once again, their area and radius is determined, and the size distribution is computed. Also, their radial pair correlation function is computed, and a binary file of particle coordinates is written, to be read by a rendering program we call Balls, and by the analysis program HexDomains.

Hexagonal domains. The hexagonally packed domains are now be enumerated and quantified using a program called HexDomains, which determines a wide variety of structural parameters from the array of particle coordinates. The first step is the determination of the neighbors of each of the particles. Neighbors determination is an N^2 problem when approached in a straightforward way, but we have developed a fast, linear-N algorithm that for N=10,000 particles accomplishes this task in much less than a second on a typical desktop computer.

The next step in the analysis is the determination of the type of location in which a particle resides. There are many possible categories, principal of which are hexagonal

sites, hexagonal edge sites, hexagonal defect sites at the boundaries of hexagonal domains of different orientation, and stacked hexagonal sites, a category that applies only to those cases where 3-D information is available, such as in simulations of crystal formation. The site type determination is based on complex criteria, including the number of neighbors, "bond" angles, etc.

The crystalline domains are then determined by a type of multidimensional percolation. In the normal percolation problem neighbors are defined by physical proximity alone. It is possible to include other criteria to determined bonding, and we stipulate the particle orientations also agree within a small acceptable amount, typically about 3°. The particle orientation is defined for hexagonal particles by the angle, between -30° and +30°, needed to rotate the crystal in which the particle resides so that contacting chains of hexagonal spheres align with the y (vertical) axis. The result of this percolation process is the enumeration of all the crystalline domains in the array.

Lattice spacing. Once the crystalline domains are determined it is possible to accurately compute the lattice spacing of the array. One simple approach to this problem, that works well only for high quality arrays, is to compute the radial or vector pair correlation function of the particle centers of mass alone. This is an improvement on a diffraction experiment, because the diffraction pattern is convoluted with the particle form factor (a Bessel function for a sphere), but with image processing it is possible to do better still, by excluding particles that are not in hexagonal sites, such as those at domain boundaries etc., and by excluding interdomain correlations.

The *intradomain* correlation function is computed by orienting each domain so that chains of hexagonal particles lie along the y (i.e. vertical) axis. This results in the vector pair correlation function of **Fig. 4**. It is possible to obtain accurate values of the lattice spacing from these data. For disordered lattices substantially more disordered than the example given here, the intradomain function can be substantially better than the total function, which might only appear as a few diffuse rings with poor signal to noise, due to the large incoherent background caused by the disordered regions. The particle gaps, determined by the choice of capping agent, can be determined by subtracting the average particle diameter from the lattice spacing.

References

1. Boutonnet, A.; Kizling, J.; Stenius, P.; Maire G. *Colloids and Surfaces*, **1982**, *5*, 209-225.
2. Wilcoxon, J. P.; Williamson, R. L. Proceedings of the Fall Materials Research Society, Boston, MA **1989**.
3. Wilcoxon, J. P.; Williamson, R. L. *J. Chem. Phys.* **1993**, *98*, 9933-9950.
4. Wilcoxon, J. P.; Provencio, P. P. *J. Phys. Chem. B* **1999**, *103*, 9809-9812.
5. Giersig, M.; Mulvaney, P. *J. Phys. Chem.* **1993**, *97*, 6334-6336.
6. Enustun, B. V.; Turkevich, J. *J. Amer. Chem. Soc.* **1963**, *85*, 3317.
7. Brust, M.; Walker, M.; Berthell D.; Schiffrin D. J.; Whyman, R. *J. Chem. Soc., Chem Comm.* **1994**, 801-802.
8. Leff, D. V.; Ohara, P. C.; Heath, J. R.; Gelbart, W. M. *J. Chem. Phys.* **1995**, *99*, 7036-7041.
9. Whetten, R. L.; Khoury, J. T.; Alvarez, S. M.; Murthy, S.; Vezmar, I.; Wang, Z. L.; Stephens P. W.; Cleveland, C. L.; Luedtke, W. D.; Landman, U. *Adv. Mater.*. **1996**, *8*, 428-433.
10. Ohara, P. C.; Leff, D. V.; Heath, J. R.; Gelbart, W. M. *Phys. Rev. Lett.* **1995**, *75*, 3466-3469.
11. Sarathy, K. V.; Raina, G.; Yadav, R. T.; Kulkarni, G. U.; Rao, C. N. R.; *J. Phys. Chem. B* **1997**, *101*, 9876-9880.
12. Korgel, B. A.; Fullam, S.; Connolly, S.; Fitzmaurice, D. *J. Phys. Chem.* **1998**, *102*, 6579-6588.
13. Taleb, A.; Petit, C.; Pileni, M. P. *J. Chem. Phys. B* **1998**, *102*, 2214-2220.
14. Brust, M.; Berthell D.; Schiffrin D. J.; Kiely, C. J. *Adv. Mater.*. **1995**, *7*, 795-797.
15. Andres, R. P.; Bielefeld, J. D.; Henderson, J. I.; Janes, D. B.; Kolagunta, V. R.; Kubiak, C. P.; Mahoney, W. J.; Osifchin, R. G. *Science* **1996**, *273*, 1690-1693.
16. Fink, J.; Kiely, J.; Bethell, D.; Schiffrin, D. J. Chem. Mater. **1998**, *10*, 922-926.
17. We are unable to repeat this synthesis with R larger than C_{12}, because these surfactants do not make inverse micelles in toluene, even in the presence of the Au salt. In fact, for R groups larger than C_8, these surfactants do not form micelles

without the Au salt. It is possible a cosurfactant had been added to their solutions, but typical cosurfactants such as hexanol does not lead to micelle formation.

18. Buchalter, B. J.; Bradley, R. M. J. Phys. A Letters **1992**, *25*, L1219; Buchalter, B. J.; Bradley, R. M. Phys. Rev. A **1992**, *46*, 3046; Buchalter, B. J.; Bradley, R. M. J. Europhys. Letters **1994**, *26*, 159.

Table I

Solution compositions for selected Pd nanoclusters

Sample	Salt	Surfactant	Oil	Reducing Agent	R	Thiol
Pd 149	Na_2PdCl_4	C12E5	C16	2.0 M $LiBH_4$	4	C12SH
Pd 153	Na_2PdCl_4	C12E5	C16	2.0 M $LiBH_4$	4	C6→C18SH

Table II

Solution compositions for selected Pt nanoclusters

Sample	Salt	Surfactant	Oil	Reducing Agent	R	Thiol
Pt 58	H_2PtCl_6-$6H_2O$	C12E5	C8	2.0 M $LiBH_4$	4	C12SH
Pt 76	Na_2PtCl_6-$6H_2O$	C12E4	C8	2.0 M $LiBH_4$	4	hydrophilic
Pt 78	Na_2PtCl_6-$6H_2O$	C12E4	C10	2.0 M $LiBH_4$	4	C6→C16SH
Pt 98	H_2PtCl_6-$6H_2O$	C12E6	C8	0.2 M $LiBH_4$/THF	4	C12SH
Pt 119	H_2PtCl_6-$6H_2O$	C12E5	C10	2.0 M $LiBH_4$	4	C12SH
Pt 160	H_2PtCl_6-$6H_2O$	C12E5	C8	0.2 M $LiBH_4$/THF	4	C12SH, 1 h, 1 d, 1 wk
Pt 161	H_2PtCl_6-$6H_2O$	C12E5	C8	0.2 M $LiBH_4$/THF	2	C12SH, 1 h, 1 d, 1 wk
Pt 162	H_2PtCl_6-$6H_2O$	C12E5	C8	0.2 M $LiBH_4$/THF	1	C12SH, 1 h, 1 d, 1 wk
Pt 165	H_2PtCl_6-$6H_2O$	C12E5	C8	0.2 M $LiBH_4$/THF	4	C3→C8SH, 24 hrs
Pt 178	H_2PtCl_6-$6H_2O$	C12E5	C8	0.2 M $LiBH_4$/THF	4	C6→C18SH, 24 hrs

Table III

QELS results for hydrophilic capping ligands

Capping Ligand	dimethyl formamide	formamide	n-methyl formamide
3-mercapto-1-propanesulfonic acid, Na salt	C	A	A
2-mercaptoethanesulfonic acid, Na salt	C	A	A
2-mercaptoethanol	B	B	B
3-mercaptopropionic acid	C	B	B
thiodiglycolic acid	B	-	A
2,2'-thiodiethanol	C	B	A
3,3'-thiodipropanol	B	A	B
(3-mercaptopropyl)trimethoxysilane	B	A	A
thioglycerol	C	B	B
1-mercapto-2-propanol	B	B	B

A = single nanocluster hydrodynamic radius; B = good appearance; C = precipitates

Figure Captions

Fig. 1. The freshly synthesized **Pd 149** nanoclusters are sufficiently polydisperse that superlattices do not form (top). Analysis of this image yields a number-average cluster diameter of 3.9nm ± 25%. After annealing for 96 hrs at 70°C the clusters have ripened considerably, yielding a number average cluster diameter of 5.6 nm ± 16%.

Fig. 2. The tendency for Pt nanoclusters to develop faceted surfaces is very strong, as seen in this 100kx TEM of **Pt 78** (top). Remarkably, the faceted particles are single crystals, as revealed by the lattice fringes observed in high resolution 600kx TEM (bottom).

Fig. 3. Highly faceted particles of **Pt 119** form a mosaic upon solvent evaporation on a holey carbon TEM grid. Stacks of high aspect ratio rectangles can be seen throughout this image. Simulated annealing studies of dense packed objects routinely demonstrate mosaic formation, as the system is forced to minimize its area as the solvent evaporates.

Fig. 4. TEM of a 2-D superlattice of 4.0nm±10% **Pt 98A** nanoclusters capped with dodecanethiol (top). The intradomain vector pair correlation function of the particle centers of mass enables an accurate determination of the lattice spacing (bottom).

Fig. 5. Distribution of particle diameters for **Pt 98A** is well fit to a Gaussian to obtain the number-average particle diameter and standard deviation.

Fig. 6. High resolution TEM of freshly synthesized **Pt165** indicates a particle size of 2.7nm.

Fig. 7. Bilayers of alkanethiol capped **Pt 165** (top) and **Au 646** nanoclusters (bottom) show an interesting difference. Au nanoclusters tend to sit in the 2-fold saddle sites, whereas Pt nanoclusters sit in the 3-fold saddle sites. The scale is the same in these HRTEM images, taken at 400kx..

Fig. 8. High resolution TEM of a single domain of a 3-D superlattice of 2.7 nm **Pt 165** nanoclusters capped with an alkanethiol (top). Electron diffraction image (bottom).

Fig. 9. The size distribution of **Pt 58A** is narrow for platinum, nearly as good as the best Au nanoclusters we have synthesized. The long aging time is a key factor in producing narrow dispersity Au nanoclusters.

Fig. 10. A surprising aspect of the **Pt 58A** sample is that 2-D arrays often form as square lattices instead of hexagonal.

Fig. 11. Optical micrograph (top) of 10 micron superlattice crystals of **Pt 58A** grown on silicon, and an SEM of a single crystal (bottom).

Fig. 12. Optical micrograph (top) of superlattice crystals of **Pt 58A** that are possibly twinned.

Fig. 13. Optical image (1250x) of quasi-hexagonal superlattice crystals of **Pd 149**. Substrate was put in 70°C oven to speed crystallization.

Fig. 14. Pt 178 clusters show an increase in the interparticle spacing of 1.4 Å per carbon of the alkanethiol. Errors bars are obtained from the width at half height of the first peak of the pair correlation function. These nanoclusters have a diameter of 3.54nm±13%.

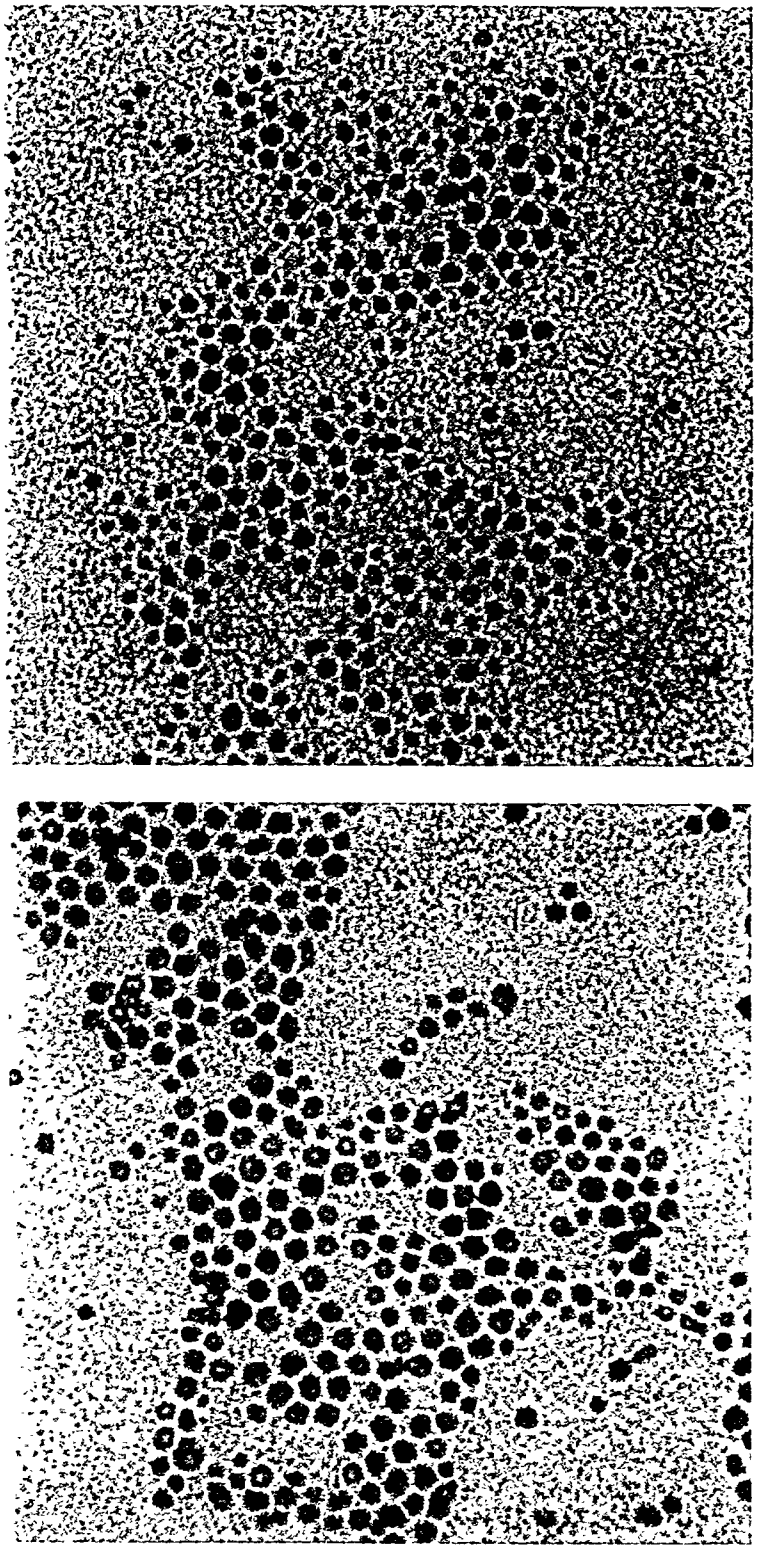

Figure 1 Martin et al

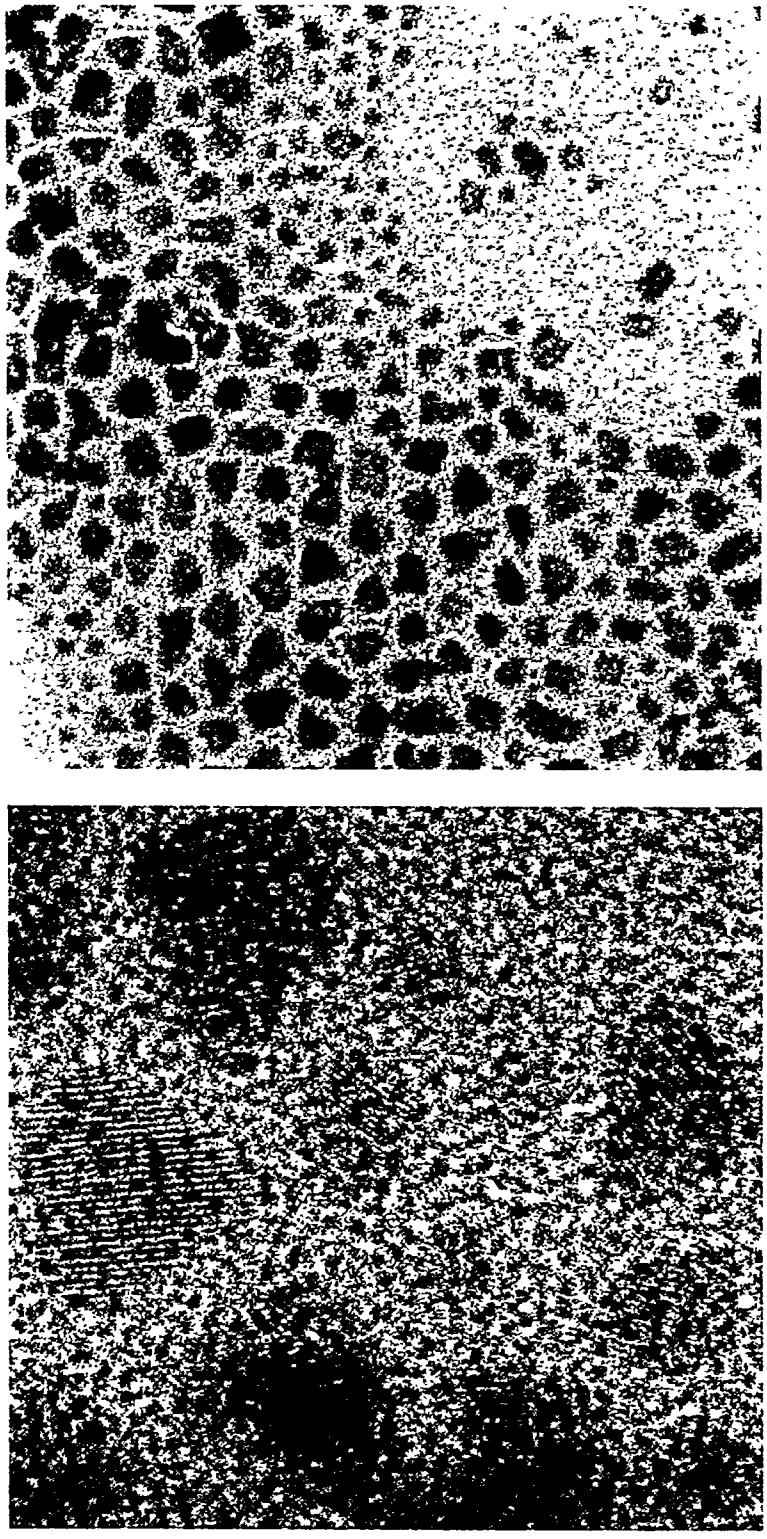

Figure 2 Martin et al

Figure 3 Martin et al

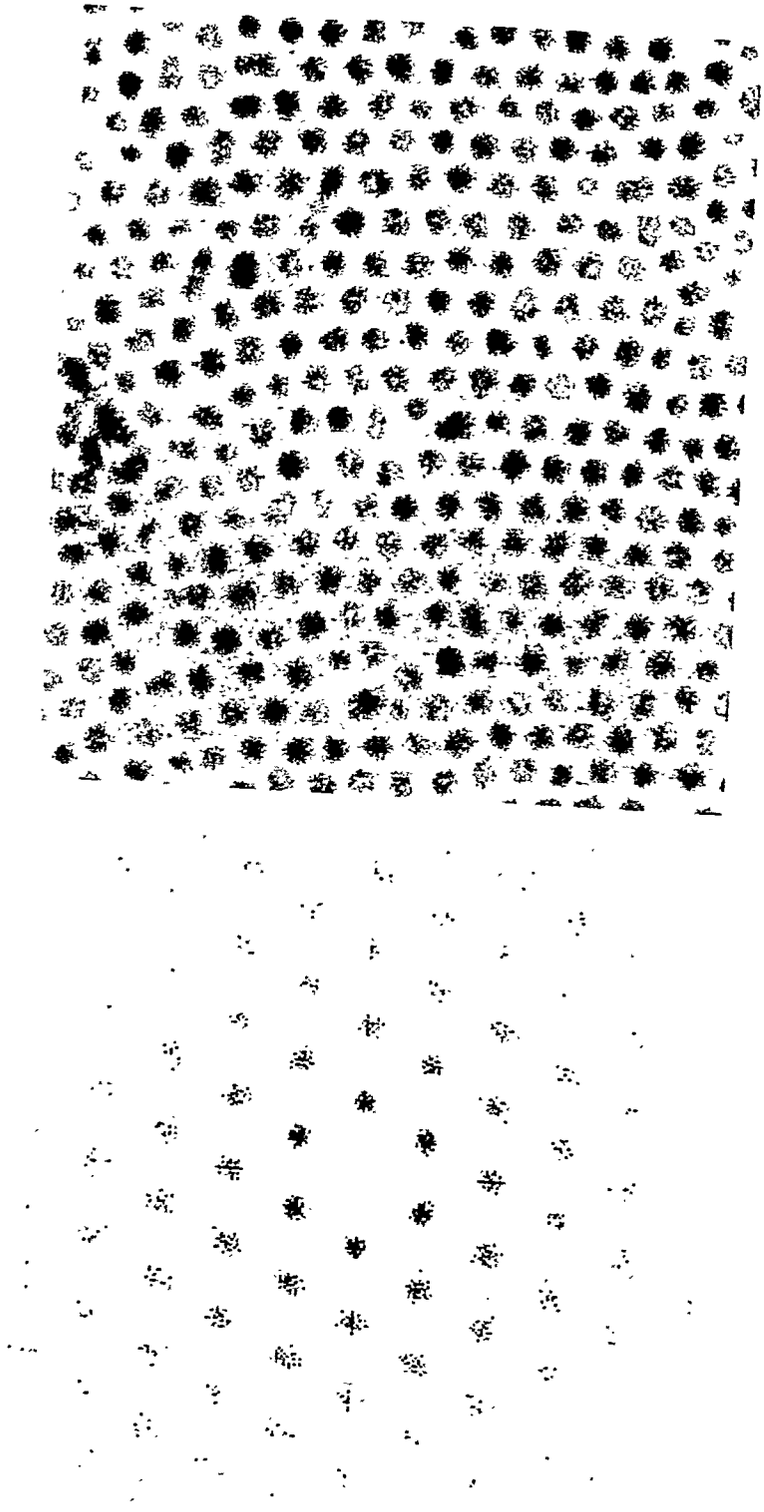

Figure 4 Martin et al

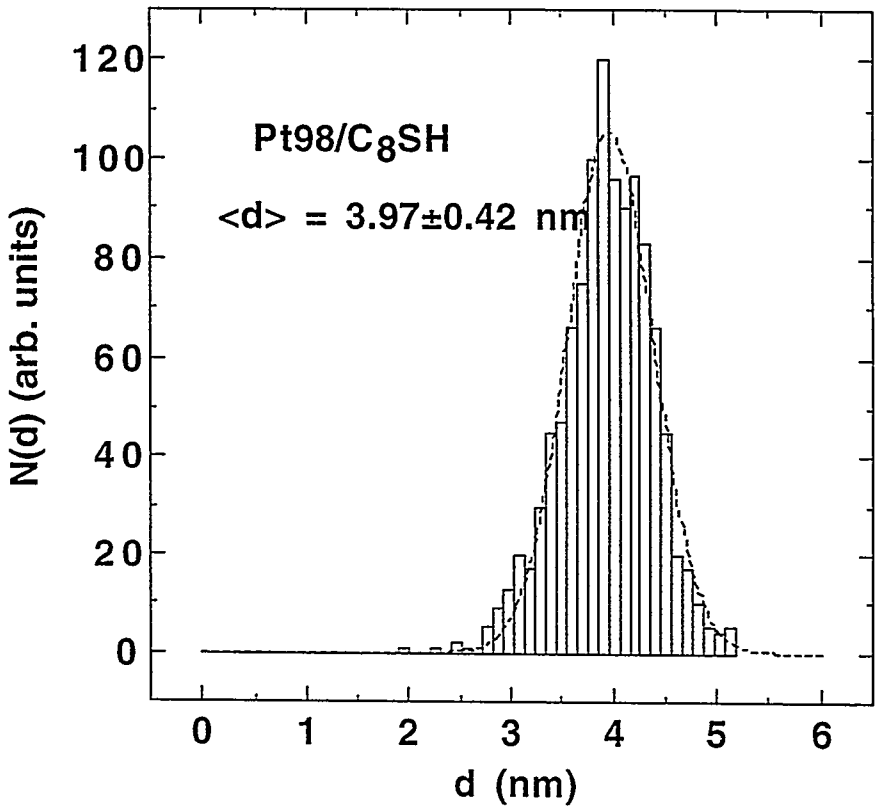

Figure 5 Martin et al

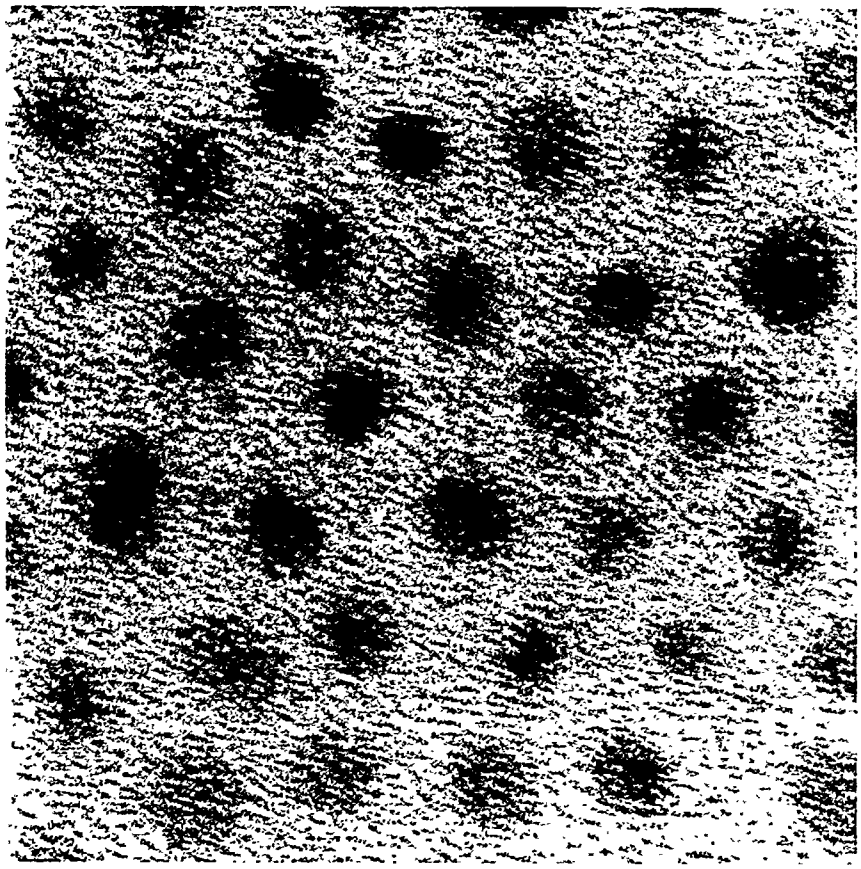

Figure 6 Martin et al

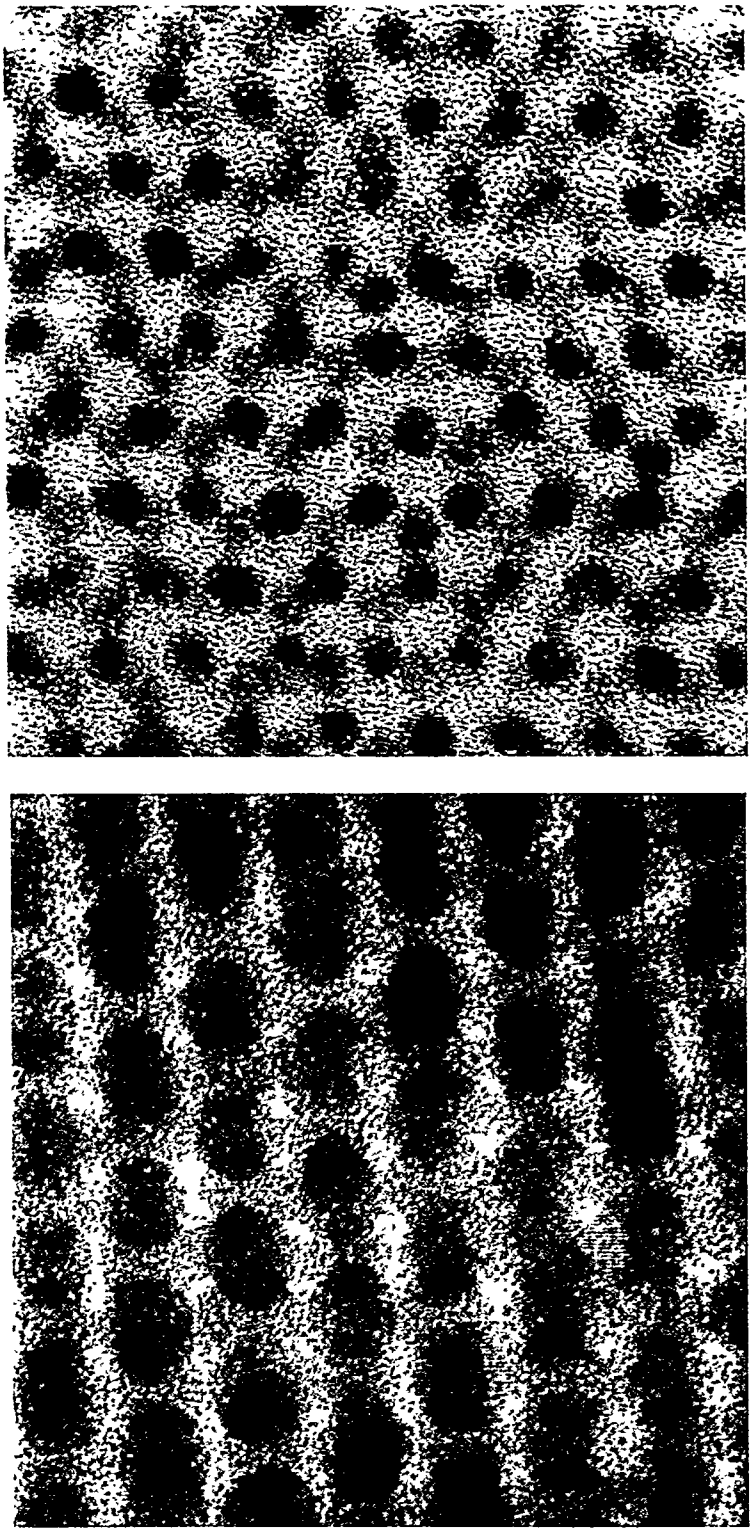

Figure 7 Martin et al

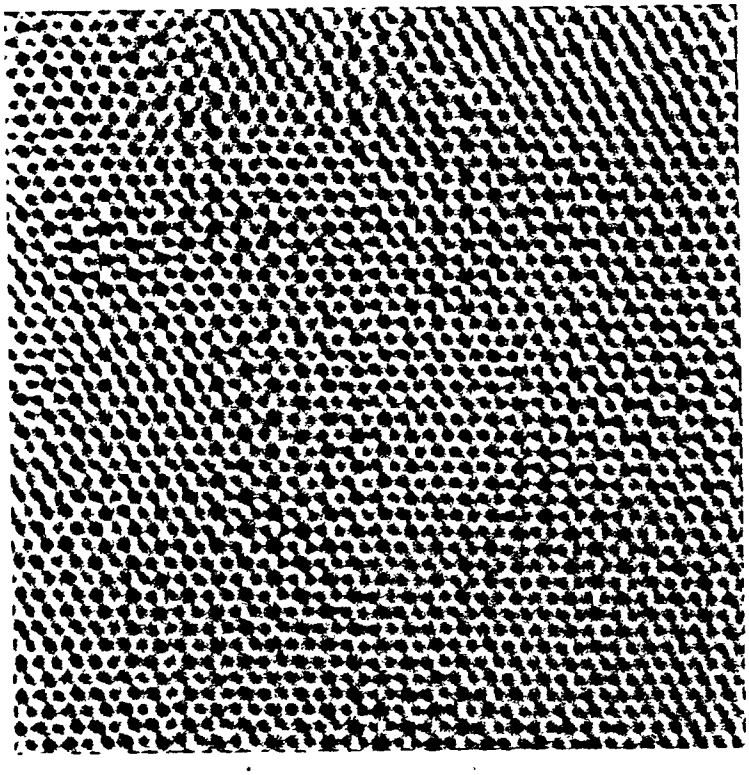

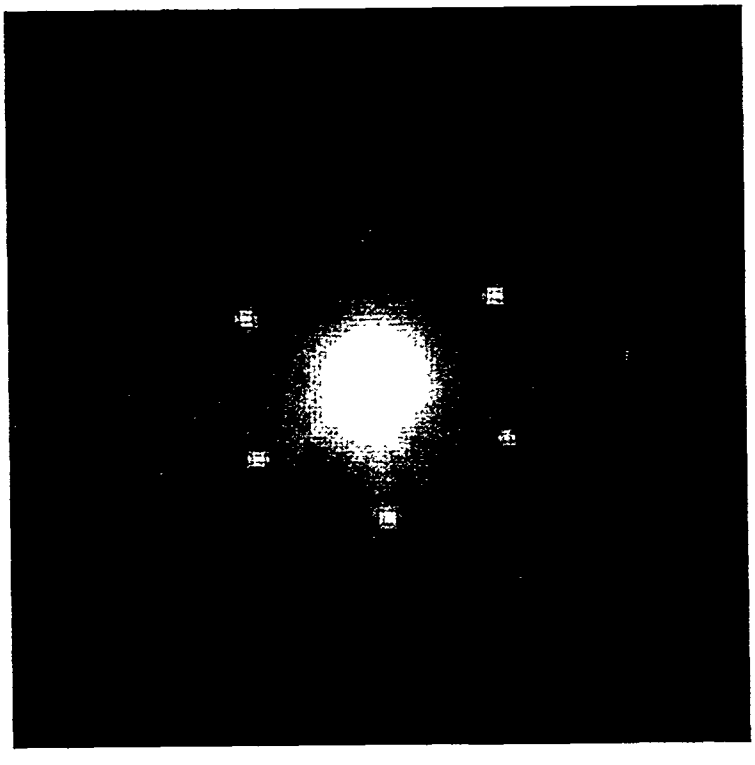

Figure 8 Martin et al

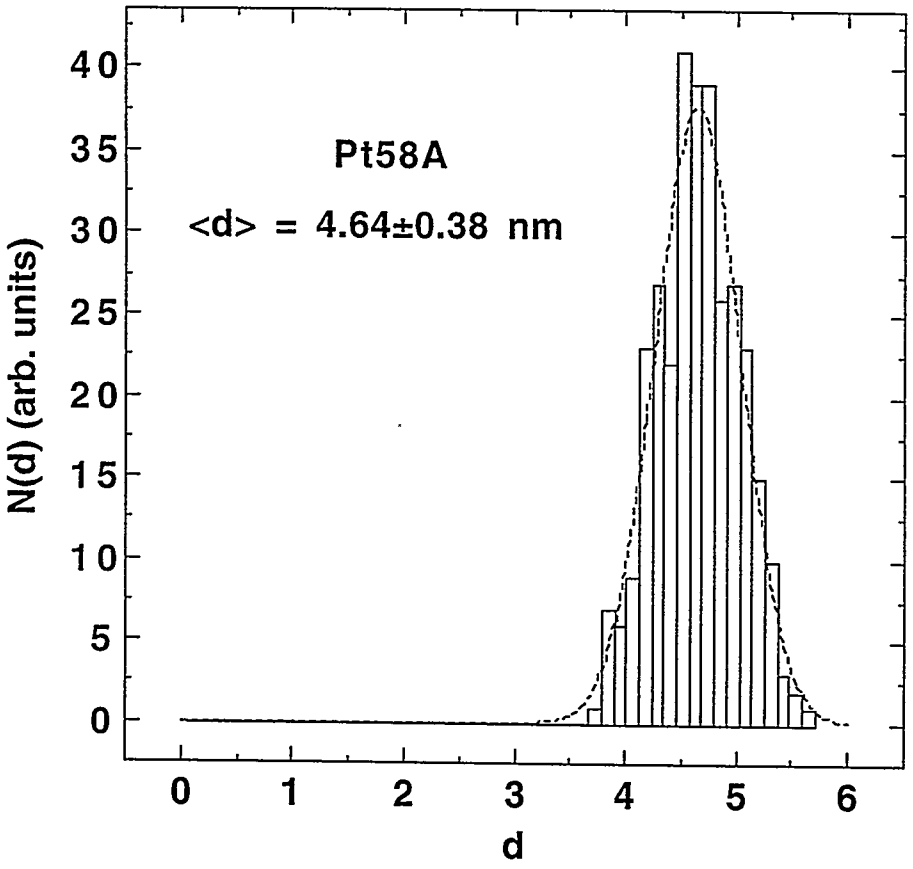

Figure 9 Martin et al

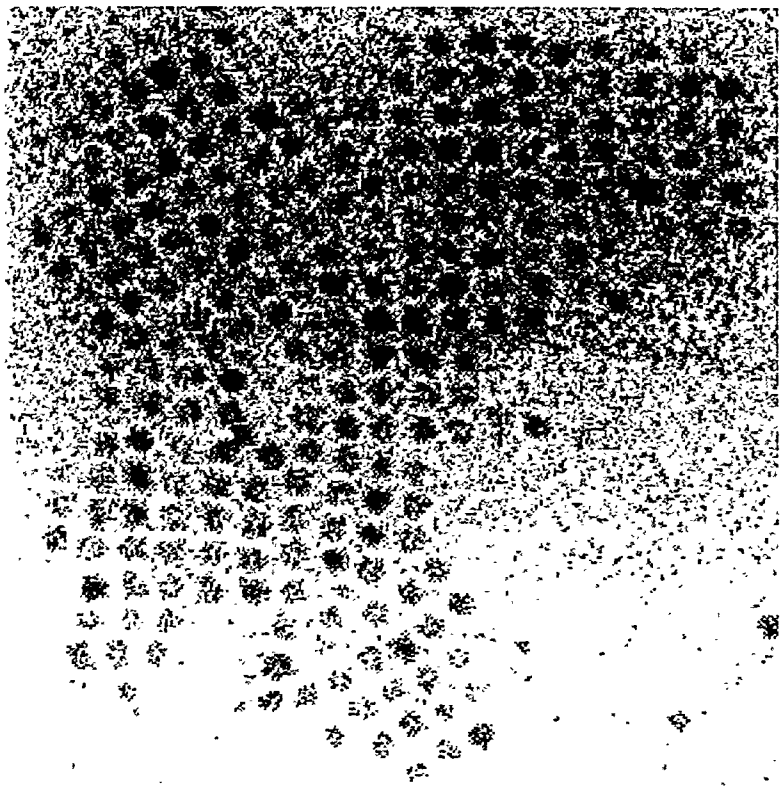

Figure 10 Martin et al

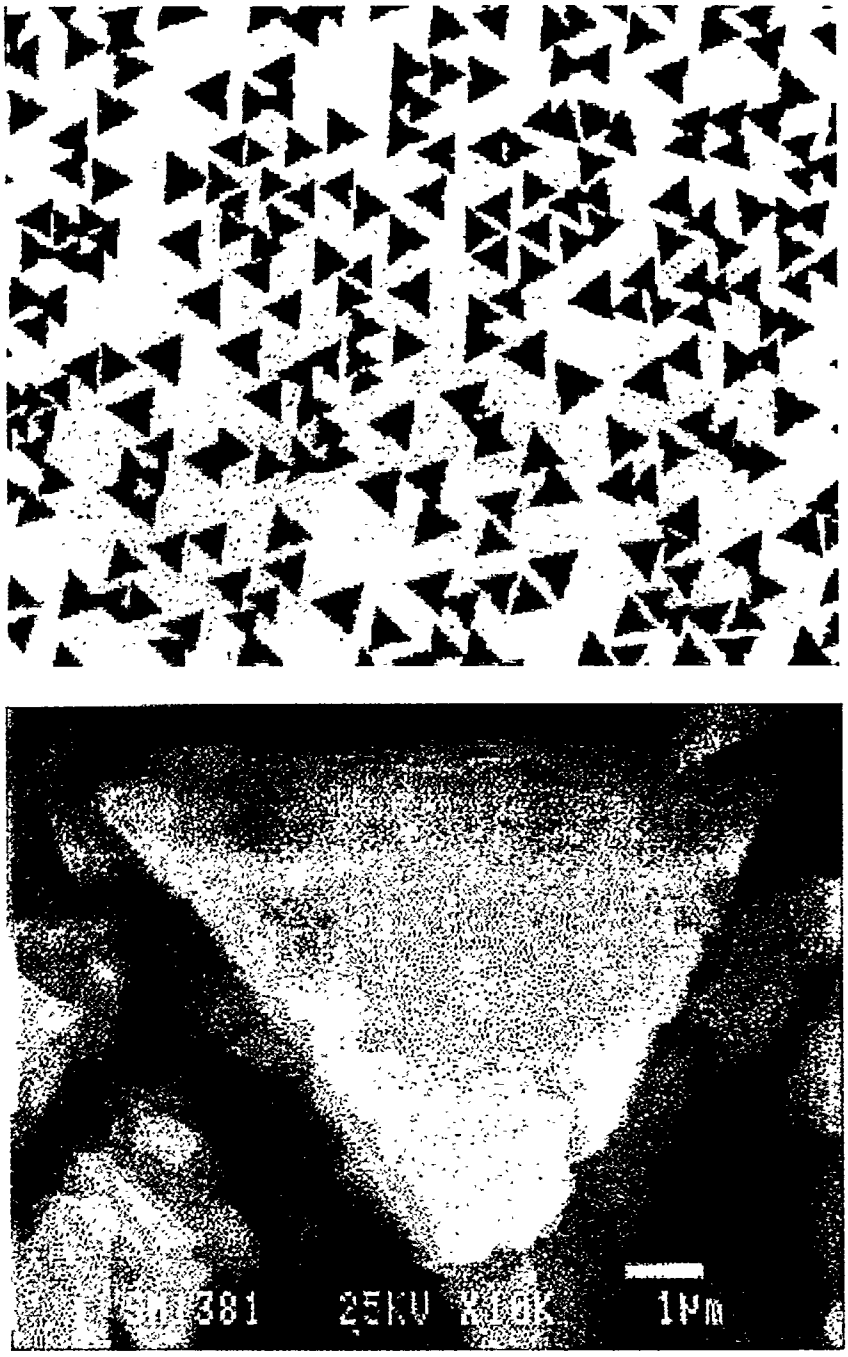

Figure 11 Martin et al

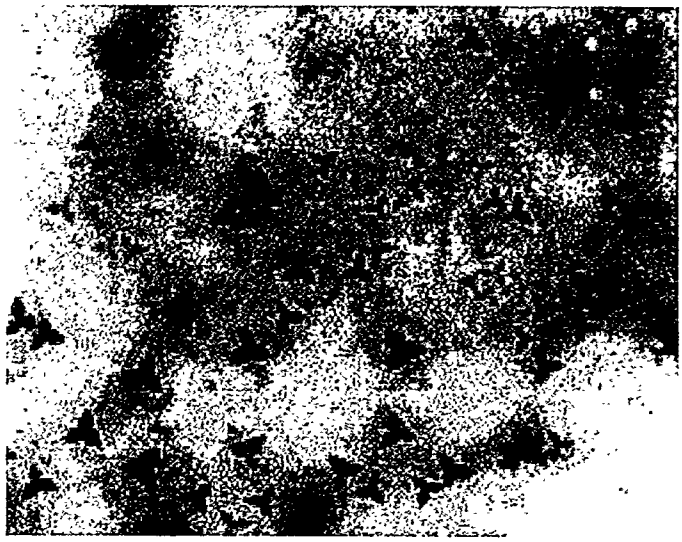

Figure 12 Martin et al

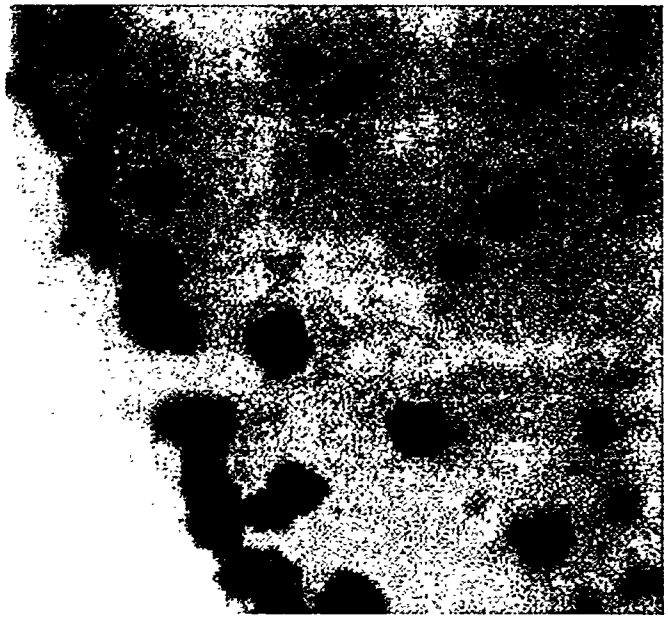

Figure 13 Martin et al

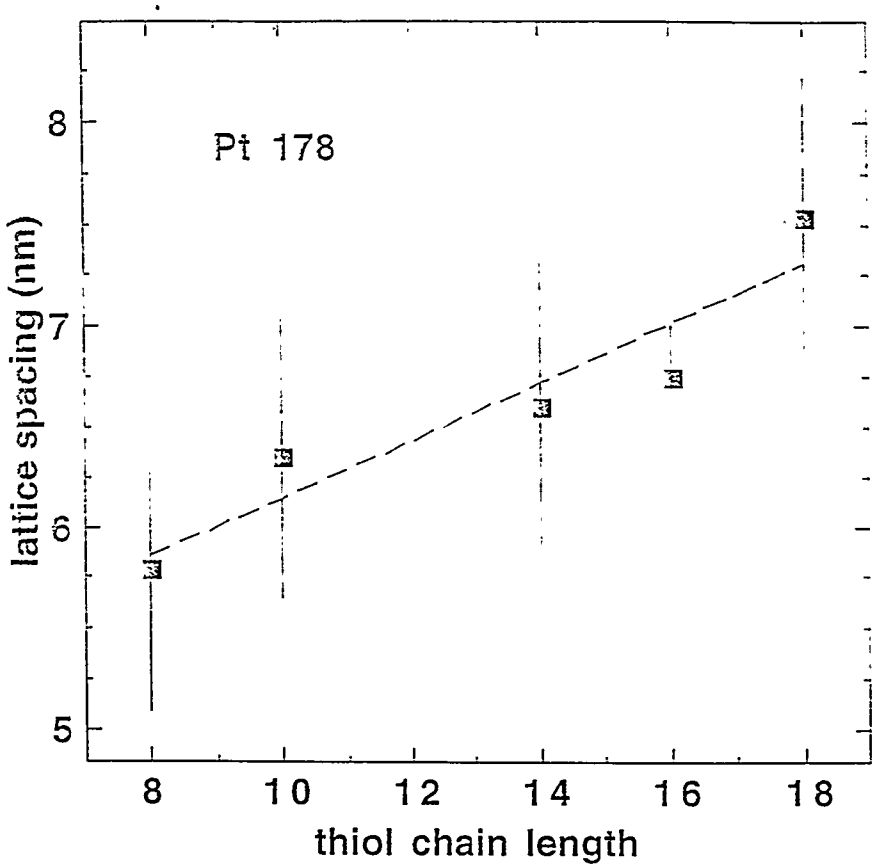

Figure 14 Martin et al